INTERNATIONAL JOURNAL FOR NUMERICAL METHODS IN FLUIDS
Int. J. Numer. Meth. Fluids 2006; **52**:1247–1275
Published online 19 June 2006 in Wiley InterScience (www.interscience.wiley.com). DOI: 10.1002/fld.1249

Study of techniques for obtaining continuous models from 2D discrete reduced-order state-space CFD models

Ann L. Gaitonde*,† and D. P. Jones

Department of Aerospace Engineering, University of Bristol, University Walk, Bristol BS8 1TR, U.K.

SUMMARY

The application of unsteady computational fluid dynamics (CFD) codes to aeroelastic calculations leads to a large number of degrees of freedom making them computationally expensive. Reduced-order models (ROMs) have therefore been developed; an ROM is a system of equations which is able to reproduce the solutions of the full set of equations with reasonable accuracy, but which is of lower order. ROMs have been the focus of research in various engineering situations, but it is only relatively recently that such techniques have begun to be introduced into CFD. In order for the reduced systems to be generally applicable to aeroelastic calculations, it is necessary to have continuous time models that can be put into discrete form for different time steps. While some engineering reduction schemes can produce time-continuous models directly, the majority of methods reported in CFD initially produce discrete time or discrete frequency models. Such models are restricted in their applicability and in order to overcome this situation, a continuous time ROM must be extracted from the discrete time system. This process can most simply be achieved by inverting the transformation from continuous to discrete time that was initially used to discretize the CFD scheme. However an alternative method reported in literature is based on continuous time sampling, even when this is not used for the initial discretization of the CFD code. This paper focuses on one particular method for ROM generation, eigensystem realization algorithm (ERA), that has been used in the CFD field. This is implemented to produce a discrete time ROM from a standard CFD code, that can be used to investigate methods for obtaining continuous ROMs and the limitations of the resulting models. Copyright © 2006 John Wiley & Sons, Ltd.

Received 25 August 2005; Revised 29 March 2006; Accepted 31 March 2006

KEY WORDS: reduced order; unsteady CFD; ERA

1. INTRODUCTION

Many engineering and scientific problems involve the solution of a set of differential equations. In situations where there are a large number of degrees of freedom, solving this set of equations is

*Correspondence to: Ann L. Gaitonde, Department of Aerospace Engineering, University of Bristol, University Walk, Bristol BS8 1TR, U.K.
†E-mail: ann.gaitonde@bris.ac.uk

computationally expensive. One example of this is in the modelling of the stability and responses of flexible fixed wing aircraft. Theoretical prediction of the unsteady flows requires models of both the fluid motion and the structure. The focus in this paper is only on the modelling of the *fluid* motion, however the methods described here are general and are also applicable to other dynamic systems.

Accurate fluid models for prediction of unsteady flow features for aeroelastic calculations require solution of the full unsteady non-linear Euler or Navier–Stokes equations (see for example References [1–5]). However, such methods are too computationally expensive for use in industry. This is due to the fact that many thousands of parameter variations must be investigated. Therefore, historically there has been a reliance on simpler methods which are not able to predict all the features encountered in the flight regime of modern aircraft. More recently research has been directed towards the application of system reduction methods, developed in other fields of engineering to fluid modelling. The objective of a reduced-order model (ROM) is to identify a lower cost model from the full system of equations, while still retaining reasonable accuracy. For an extensive review of fluid motion modelling from classical methods through to recent developments see Reference [6].

In this work, the flow under investigation is assumed to be statically non-linear, but dynamically linear. The assumption of dynamic linearity is a common approach used in the development of ROMs and is a good approximation in many situations e.g. flutter calculations. While many reduction methods can be directly applied to the matrices of the large linear system of equations (e.g. eigensystem realization algorithm (ERA) (modified Ho algorithm) [7, 8], POD [9], Krylov-subspace [10], Arnoldi [11, 12]), in fluid dynamics it has been more common to create ROMs in the discrete frequency or discrete time domain using methods that do not require explicit construction of the system matrices. This is because in general for most CFD codes neither the continuous nor the discrete system matrices are ever explicitly constructed. Instead the CFD code solves either a discrete frequency or discrete time approximation to the continuous time set of equations (obtained after spatial discretization); the ROM initially produced is therefore itself a discrete frequency or discrete time model.

Reduced systems have then been found by a number of techniques when the flow is assumed harmonic with a discrete frequency, most prominently via eigenmode summation and proper orthogonal decomposition [13]. Eigenmode summation has been used to reduce the Euler [14] equations. However, the application of proper orthogonal decomposition is increasingly investigated with models constructed for the Euler equations by Hall *et al*. [15, 16]. Further improvements via balanced proper orthogonal decomposition [17] have also been obtained.

An alternative approach, identifies the discrete time pulse responses of the CFD code, which characterize all solutions of the dynamically linear system [18–20]. These responses are then used with the ERA [7] to obtain an ROM. ERA is an SVD-based method [21, 22] and has links to POD, see Reference [23] where both ERA and POD are applied to the same problem. The ERA method can be applied with minimal work to existing CFD codes and is the approach taken in this study to obtain discrete time models.

The above discrete models are restricted to a fixed frequency or fixed time step, which means that the discrete ROM cannot be accurately coupled to structural models with discrete non-linearities (such as freeplay in a control surface). A time continuous ROM does not have this restriction [24]. This focus of this paper is then to examine and compare methods for deriving a continuous time ROM of the *fluid* from a discrete time ROM.

The CFD code used as the basis for this work is an unsteady dual-time finite-volume scheme which solves the non-linear Euler equations on a moving mesh [5]. The mean or base solution is

DOI: 10.1002/fld

found by running the code in steady flow mode (i.e. flow is statically non-linear). The dynamically linear pulse responses can be found by time-linearizing the code [25, 26] and performing a series of calculations for pulse inputs [27]. An alternative method which approximates the linear pulse response as the linear portion of the non-linear response of the full non-linear code has been used by Silva [19]. In this latter case, twice as many pulse response calculations must be performed. Here, the first approach has been adopted.

2. CONTINUOUS LINEAR EULER EQUATIONS

The dynamically linear responses, about the non-linear mean solution, are calculated using the 2D linearized Euler equations (also sometimes called the small disturbance Euler equations) on moving meshes [26]. This description of the ROM generation method, starts from a spatially discrete, but time continuous version of the linearized Euler equations. (Note that the CFD code ultimately used is fully discrete in both time and space.) For simplicity, throughout the rest of this paper references to continuous or discrete models/systems indicate only the time-dependent nature of the system.

These equations can be applied to any motion where the perturbations are small. As an example, if these equations are applied to calculations of the flow about 2D aerofoils with trailing edge flaps, that can undergo linearized pitch motions [26], then the non-dimensional system can be rewritten in continuous state-space form, more useful for this study as

$$\begin{aligned} \dot{\mathbf{x}}(t) &= \mathbf{A}\mathbf{x}(t) + \mathbf{B}\mathbf{u}(t) \\ \mathbf{y}(t) &= \mathbf{C}\mathbf{x}(t) + \mathbf{D}\mathbf{u}(t) \end{aligned} \tag{1}$$

$\mathbf{A}$, $\mathbf{B}$, $\mathbf{C}$ and $\mathbf{D}$ are the system matrices. The input vector $\mathbf{u}$ and the state-vector $\mathbf{x}$ are given by

$$\begin{aligned} \mathbf{u} &= [\alpha, \delta, \dot{\alpha}, \dot{\delta}]^{\mathrm{T}} \\ \mathbf{x} &= [\hat{\rho}_{2,2}, \hat{u}_{2,2}, \hat{v}_{2,2}, \hat{p}_{2,2} \ldots \hat{\rho}_{i_{\max}, j_{\max}}, \hat{u}_{i_{\max}, j_{\max}}, \hat{v}_{i_{\max}, j_{\max}}, \hat{p}_{i_{\max}, j_{\max}}]^{\mathrm{T}} \end{aligned} \tag{2}$$

α is the pitch angle, δ is the flap angle, $\hat{\rho}$, $\hat{u}$, $\hat{v}$ and $\hat{p}$ are the changes from the mean values of the density, speeds and pressure. Note that the scheme considered here is a cell-centred one, with centres inside the computational domain labelled $i = 2, i_{\max}$, $j = 2, j_{\max}$.

The vector $\mathbf{y}$ is the output and is defined to produce the required information about the linear system. An example of a suitable $\mathbf{y}$ for the motion defined above is

$$\mathbf{y} = [\hat{C}_l, \hat{C}_m, \hat{C}_h]^{\mathrm{T}} \tag{3}$$

where $\hat{C}_l$, $\hat{C}_m$ and $\hat{C}_h$ are the perturbations in the lift, pitching moment and hinge moment coefficients from the mean values.

The differential equation (1) is solved by multiplying through by $\mathrm{e}^{-\mathbf{A}t}$, regrouping terms and then integrating from 0 to t

$$\begin{aligned} \mathbf{x}(t) &= \mathbf{\Phi}(t)\mathbf{x}(0) + \int_0^t \mathbf{\Phi}(t-\tau)\mathbf{B}\mathbf{u}(\tau)\,\mathrm{d}\tau \\ \mathbf{y}(t) &= \mathbf{C}\mathbf{\Phi}(t)\mathbf{x}(0) + \int_0^t \mathbf{C}\mathbf{\Phi}(t-\tau)\mathbf{B}\mathbf{u}(\tau)\,\mathrm{d}\tau + \mathbf{D}\mathbf{u}(t) \end{aligned} \tag{4}$$

DOI: 10.1002/fld

where $\mathbf{\Phi}(t) = e^{\mathbf{A}t}$. The first term on the right-hand side is the free response (i.e. the response when $\mathbf{u} = 0$) and the remaining terms are called the forced response (i.e. the response when $\mathbf{x}(0) = 0$ and $\mathbf{u}(t) \neq 0$). In the linearized Euler equations $\mathbf{x}(0) = 0$ so, provided the entries of $\mathbf{Du}(t)$ are continuous for $t > 0$, the total response can be written as

$$\begin{aligned} \mathbf{x}(t) &= \int_0^t \mathbf{\Phi}(t-\tau)\mathbf{B}\mathbf{u}(\tau)\,\mathrm{d}\tau \\ \mathbf{y}(t) &= \int_0^t (\mathbf{C}\mathbf{\Phi}(t-\tau)\mathbf{B} + \mathbf{D}\delta(t-\tau))\mathbf{u}(\tau)\,\mathrm{d}\tau \end{aligned} \tag{5}$$

An alternative expression for the output $\mathbf{y}(t)$ is

$$\mathbf{y}(t) = \int_0^t \mathbf{H}(t-\tau)\mathbf{u}(\tau)\,\mathrm{d}\tau \tag{6}$$

The continuous-time impulse response matrix $\mathbf{H}(t)$ has, as its ith column, the output response of the system for a unit impulse input $\delta(t)$ on the ith component of $\mathbf{u}$ with all other inputs set to zero. If this function, $\mathbf{H}(t)$, and its derivatives could be identified, then it would be possible to construct a generalized Hankel matrix of the system [28] and identify directly an ROM of the continuous system using ERA. However, in the case of the linearized Euler equations, the information required to construct this matrix is not directly available.

3. A DISCRETE TIME CFD MODEL OF THE CONTINUOUS SYSTEM

A continuous ROM of the continuous linearized Euler equations is therefore found indirectly. The continuous equations are put into a discrete form that allows the terms required to construct a discrete Hankel matrix of the system to be easily identified. A one-step implicit finite difference scheme is used for the time derivative as this permits direct identification of the Markov parameters which form the required terms of the Hankel matrix. The one-step scheme, in this case, acts a simple filter of the eigenvalues of the continuous system to allow dominant low-frequency terms to be identified and retained in the reduced-order system. The continuous ROM ultimately obtained can be put into discrete form using any appropriate finite difference approximation scheme. Note also that an approximate linear response can be extracted from two calculations using a non-linear CFD code, so the current method can be applied directly to existing schemes [19, 29]. The discrete form of Equation (1) is

$$\begin{aligned} \frac{\tilde{\mathbf{x}}_k - \tilde{\mathbf{x}}_{k-1}}{\Delta t} &= \mathbf{A}\tilde{\mathbf{x}}_k + \mathbf{B}\tilde{\mathbf{u}}_k \\ \tilde{\mathbf{y}}_k &= \mathbf{C}\tilde{\mathbf{x}}_k + \mathbf{D}\tilde{\mathbf{u}}_k \end{aligned} \tag{7}$$

where $\tilde{\mathbf{x}}$, $\tilde{\mathbf{u}}$ and $\tilde{\mathbf{y}}$ are discrete approximations to the state, input and output vectors respectively.

On rearranging this becomes

$$\begin{aligned} \tilde{\mathbf{x}}_k &= \tilde{\mathbf{A}}\tilde{\mathbf{x}}_{k-1} + \tilde{\mathbf{B}}\tilde{\mathbf{u}}_k \\ \tilde{\mathbf{y}}_k &= \tilde{\mathbf{C}}\tilde{\mathbf{x}}_k + \tilde{\mathbf{D}}\tilde{\mathbf{u}}_k \end{aligned} \tag{8}$$

DOI: 10.1002/fld

where the discrete system matrices are given by

$$\begin{aligned}\tilde{\mathbf{A}} &= (\mathbf{I} - \mathbf{A}\Delta t)^{-1} \\ \tilde{\mathbf{B}} &= (\mathbf{I} - \mathbf{A}\Delta t)^{-1}\mathbf{B}\Delta t \\ \tilde{\mathbf{C}} &= \mathbf{C} \\ \tilde{\mathbf{D}} &= \mathbf{D}\end{aligned} \tag{9}$$

To simplify the process of obtaining an ROM of the system, the system output is modified. Since $\mathbf{D}$ and thus $\tilde{\mathbf{D}}$ are known matrices, both the continuous system and the discrete approximation use a modified output, by subtracting the term $\mathbf{Du}(t)$ from the continuous output and the term $\tilde{\mathbf{D}}\tilde{\mathbf{u}}$ from the discrete output equation. The modified discrete system is then

$$\begin{aligned}\tilde{\mathbf{x}}_k &= \tilde{\mathbf{A}}\tilde{\mathbf{x}}_{k-1} + \tilde{\mathbf{B}}\tilde{\mathbf{u}}_k \\ \tilde{\mathbf{y}}_k^m &= \tilde{\mathbf{y}}_k - \tilde{\mathbf{D}}\tilde{\mathbf{u}}_k = \tilde{\mathbf{C}}\tilde{\mathbf{x}}_k\end{aligned} \tag{10}$$

This can be solved using one-sided z-transforms [30, 31] to give the output equation

$$\tilde{\mathbf{y}}^m(k) = \sum_{n=0}^{k} \tilde{\mathbf{H}}(k-n)\tilde{\mathbf{u}}_n \tag{11}$$

The matrix $\tilde{\mathbf{H}}(k)$ is composed of columns which are the outputs for a unit sample pulse on each input separately, i.e. the ith column is the output vector at time k for a unit sample input in the ith component of $\tilde{\mathbf{u}}$ with all other entries of $\tilde{\mathbf{u}}$ set to zero, see Reference [28].

Then if $\tilde{\mathbf{x}}_{-1} = 0$, it follows from (10) that

$$\begin{aligned}\tilde{\mathbf{y}}_0^m &= \tilde{\mathbf{C}}\tilde{\mathbf{B}}\tilde{\mathbf{u}}_0 \\ \tilde{\mathbf{y}}_1^m &= \tilde{\mathbf{C}}\tilde{\mathbf{A}}\tilde{\mathbf{B}}\tilde{\mathbf{u}}_0 + \tilde{\mathbf{C}}\tilde{\mathbf{B}}\tilde{\mathbf{u}}_1 \\ \tilde{\mathbf{y}}_2^m &= \tilde{\mathbf{C}}\tilde{\mathbf{A}}^2\tilde{\mathbf{B}}\tilde{\mathbf{u}}_0 + \tilde{\mathbf{C}}\tilde{\mathbf{A}}\tilde{\mathbf{B}}\tilde{\mathbf{u}}_1 + \tilde{\mathbf{C}}\tilde{\mathbf{B}}\tilde{\mathbf{u}}_2 \\ \tilde{\mathbf{y}}_3^m &= \tilde{\mathbf{C}}\tilde{\mathbf{A}}^3\tilde{\mathbf{B}}\tilde{\mathbf{u}}_0 + \tilde{\mathbf{C}}\tilde{\mathbf{A}}^2\tilde{\mathbf{B}}\tilde{\mathbf{u}}_1 + \tilde{\mathbf{C}}\tilde{\mathbf{A}}\tilde{\mathbf{B}}\tilde{\mathbf{u}}_2 + \tilde{\mathbf{C}}\tilde{\mathbf{B}}\tilde{\mathbf{u}}_3\end{aligned} \tag{12}$$

thus

$$\tilde{\mathbf{y}}_l^m = [\tilde{\mathbf{C}}\tilde{\mathbf{A}}^l\tilde{\mathbf{B}}, \tilde{\mathbf{C}}\tilde{\mathbf{A}}^{l-1}\tilde{\mathbf{B}}, \ldots, \tilde{\mathbf{C}}\tilde{\mathbf{A}}^2\tilde{\mathbf{B}}, \tilde{\mathbf{C}}\tilde{\mathbf{A}}\tilde{\mathbf{B}}, \tilde{\mathbf{C}}\tilde{\mathbf{B}}] \begin{bmatrix} \tilde{\mathbf{u}}_0 \\ \tilde{\mathbf{u}}_1 \\ \vdots \\ \tilde{\mathbf{u}}_{l-2} \\ \tilde{\mathbf{u}}_{l-1} \\ \tilde{\mathbf{u}}_l \end{bmatrix} \tag{13}$$

The following sequence $\mathbf{H}_k, k = 0, \infty$

$$\{\mathbf{H}_0, \mathbf{H}_1, \mathbf{H}_2, \ldots, \mathbf{H}_k, \ldots\} = \{\tilde{\mathbf{C}}\tilde{\mathbf{B}}, \tilde{\mathbf{C}}\tilde{\mathbf{A}}\tilde{\mathbf{B}}, \ldots, \tilde{\mathbf{C}}\tilde{\mathbf{A}}^k\tilde{\mathbf{B}}, \ldots\} \tag{14}$$

DOI: 10.1002/fld

is called the Markov sequence, the weighting sequence or the impulse-response sequence of the discrete system. The forced response of the discrete system is uniquely determined by its Markov sequence and the input. Thus any two systems with identical Markov sequences have identical forced responses for the same input. Note that for a system of rank n the sequence $\mathbf{H}_k,\ k=0, 2n$ defines the forced response exactly.

The system realization method described by Juang and Pappa [7] relies on being able to construct the generalized Hankel matrix whose entries are terms of the form

$$\tilde{\mathbf{C}}\tilde{\mathbf{A}}^k\tilde{\mathbf{B}} \tag{15}$$

for $k \geqslant 0$. These are available from the impulse-responses of the system, which define the Markov parameters (see Equations (11) and (13)).

The Hankel matrix in this case is the $r \times s$ block matrix given by

$$\mathbf{H}_{rs}(k) = \begin{bmatrix} \mathbf{H}_k & \mathbf{H}_{k+1} & \mathbf{H}_{k+2} & \dots & \mathbf{H}_{k+s-1} \\ \mathbf{H}_{k+1} & \mathbf{H}_{k+2} & \mathbf{H}_{k+3} & \dots & \mathbf{H}_{k+s} \\ \vdots & \vdots & \vdots & & \vdots \\ \mathbf{H}_{k+r-1} & \mathbf{H}_{k+r} & \mathbf{H}_{k+r+1} & \dots & \mathbf{H}_{k+s+r-2} \end{bmatrix} \tag{16}$$

This matrix can be used to realize and reduce the system matrices [7] via a number of different algorithms. The technique used in this study is described in the next section.

4. REALIZATION AND REDUCTION OF THE DISCRETE TIME SYSTEM

The eigenvalue realization algorithm [7] provides a method for the system matrices (continuous or discrete) to be realized or identified, provided the Hankel matrices can be constructed. This requires the Markov parameters of the system.

Focussing on the discrete system, the Markov parameters are matrices with columns equal to the value of the output vector $\tilde{\mathbf{y}}'$ for unit sample impulses on each component of $\tilde{\mathbf{u}}$ in turn. Note that the triple $[\tilde{\mathbf{A}}, \tilde{\mathbf{B}}, \tilde{\mathbf{C}}]$ is not unique and that for any non-singular matrix $\mathbf{T}$, the triple $[\mathbf{T}\tilde{\mathbf{A}}\mathbf{T}^{-1}, \mathbf{T}\tilde{\mathbf{B}}, \tilde{\mathbf{C}}\mathbf{T}^{-1}]$ is also a realization. Only a brief outline of the theory is presented here. Given that the Hankel matrices are available the next step is to carry out a singular value decomposition (SVD) of $\mathbf{H}_{rs}(0)$. It is necessary to identify the size of this matrix. If there are p outputs and m inputs to the system, then each of the Markov parameters is of size $p \times m$. Thus the size of the Hankel matrix is $rp \times sm$. Then the SVD is given by

$$\mathbf{H}_{rs}(0) = \mathbf{U}\mathbf{W}\mathbf{V}^{\mathrm{T}} \tag{17}$$

where $\mathbf{W}$ is an $sm \times sm$ diagonal matrix whose diagonal entries are called singular values which are either positive or zero, $\mathbf{U}$ is $rp \times sm$ and $\mathbf{V}$ is a $sm \times sm$ matrix. The SVD scheme is such that the elements of $\mathbf{W}$ are in size order i.e. $[w(1, 1) > w(2, 2) > w(3, 3) \cdots]$. The rank of the ROM of the system is then determined by the number of elements of $\mathbf{W}$ which are larger than some desired accuracy or by taking into account only the n largest singular values in $\mathbf{W}$. Then matrix

DOI: 10.1002/fld

$\mathbf{H}_{rs}(0)$ can be approximated as

$$\mathbf{H}_{rs}(0) = \mathbf{P}\mathbf{\Lambda}\mathbf{Q}^{\mathrm{T}} \tag{18}$$

where the matrices $\mathbf{U}$, $\mathbf{W}$, $\mathbf{V}$ have been reduced in size by deleting unnecessary columns and rows as appropriate. The reduced matrix from $\mathbf{U}$ is $\mathbf{P}: rp \times n$, the reduced matrix from $\mathbf{W}$ is $\mathbf{\Lambda}: n \times n$ and the reduced matrix from $\mathbf{V}$ is $\mathbf{Q}: sm \times n$.

It is then possible to show [7] that a realization is

$$\begin{aligned} \tilde{\mathbf{A}} &= \mathbf{\Lambda}^{-1/2}\mathbf{P}^{\mathrm{T}} H_{rs}(1)\mathbf{Q}\mathbf{\Lambda}^{-1/2} \\ \tilde{\mathbf{B}} &= \mathbf{\Lambda}^{1/2}\mathbf{Q}^{\mathrm{T}}\mathbf{E}_m \\ \tilde{\mathbf{C}} &= \mathbf{E}_p^{\mathrm{T}}\mathbf{P}\mathbf{\Lambda}^{1/2} \end{aligned} \tag{19}$$

where $\mathbf{E}_p^{\mathrm{T}} = [\mathbf{I}_p, \mathbf{0}_p, \mathbf{0}_p, \ldots, \mathbf{0}_p]$ has size $p \times rp$ and $\mathbf{E}_m^{\mathrm{T}} = [\mathbf{I}_m, \mathbf{0}_m, \mathbf{0}_m, \ldots, \mathbf{0}_m]$ has size $m \times sm$.

5. CONTINUOUS ROMs

The above scheme is used to get a discrete-time ROM of the CFD code. However, in discrete form the model is restricted to problems with a fixed time step. For problems such as aeroservoelastic modelling and non-linear structural behaviour, this limits the application of the ROMs. A time continuous ROM does not have this restriction. In this section, two methods are investigated in detail; a simple inversion of the transformation used to put the CFD code into discrete form [27] and a method based on sampling [23]. A third study be Lucia *et al*. [32] produces continuous ROMs from discrete ROMs. However, the equations as written in the paper suggest that the discrete ROM matrices $\mathbf{A}$, $\mathbf{B}$, $\mathbf{C}$ are identical to the continuous ROM matrices. This is not correct and as expected led to unstable solutions when implemented.

5.1. Inversion of the transformation

The first method considered is to invert the transformation used to get from the continuous to the discrete system (9) before system reduction. This is applied to the reduced system matrices

$$\begin{aligned} \mathbf{A} &= (\mathbf{I} - \tilde{\mathbf{A}}^{-1})/\Delta t \\ \mathbf{B} &= (\tilde{\mathbf{A}}^{-1}\tilde{\mathbf{B}})/\Delta t \\ \mathbf{C} &= \tilde{\mathbf{C}} \\ \mathbf{D} &= \tilde{\mathbf{D}} \end{aligned} \tag{20}$$

This is a valid realization of the continuous system. However, the terms which have been omitted from the reduced size discrete system Hankel matrix may not be exactly the same terms which would have been omitted from the equivalent continuous Hankel matrix. In other words, there may be some differences between a rank n continuous system ($n < \mathrm{rank}(\mathbf{A})$) obtained from the discrete system Hankel matrix and a rank n continuous system obtained directly from the continuous system Hankel matrix. However, it is shown for the test cases in this study that the dominant terms are

DOI: 10.1002/fld

correctly predicted. The continuous-system ROM could be used with different time steps and even different finite difference schemes.

5.2. *Continuous-time system with sampled inputs*

A way of obtaining a continuous system based on methods developed in the field of control and signal processing has been used by Tang *et al*. [23]. Essentially, it is an inversion of the process by which a continuous system could be put into discrete form using sampled inputs. Like the current study, Tang *et al*. did not use a sampled input method to put his system into discrete form; the sampled approach is used solely to obtain a reduced-order continuous model from a reduced-order discrete model. To explain why it might produce an adequate continuous ROM in these circumstances, consider how a system is put into discrete time using an implicit sampled input approach.

A discrete set of equations of the form

$$\begin{aligned} \tilde{\mathbf{x}}_k &= \tilde{\mathbf{A}}\tilde{\mathbf{x}}_{k-1} + \tilde{\mathbf{B}}\tilde{\mathbf{u}}_k \\ \tilde{\mathbf{y}}_k &= \tilde{\mathbf{C}}\tilde{\mathbf{x}}_k + \tilde{\mathbf{D}}\tilde{\mathbf{u}}_k \end{aligned} \tag{21}$$

is required which approximates the continuous system in the sense that the discrete output $\tilde{\mathbf{y}}(k)$ equals the continuous output $\mathbf{y}(k\Delta t)$ exactly at each sample time $k\Delta t$ for inputs that approximate the actual input. Suppose the input values of the continuous system (1) are sampled at each sample time $k\Delta t$, these values are then used to replace the continuous-system input by a stepped input

$$\mathbf{u}^*(t) = \mathbf{u}(k\Delta t) \tag{22}$$

for $(k-1)\Delta t < t < k\Delta t$. Then using Equation (4)

$$\begin{aligned} \mathbf{x}(k\Delta t) &= \int_0^{k\Delta t} \mathbf{\Phi}(k\Delta t - \tau)\mathbf{B}\mathbf{u}^*(\tau)\,\mathrm{d}\tau \\ &= \mathbf{\Phi}(\Delta t)\mathbf{x}((k-1)\Delta t) + \int_{(k-1)\Delta t}^{k\Delta t} \mathbf{\Phi}(k\Delta t - \tau)\mathbf{B}\mathbf{u}^*(\tau)\,\mathrm{d}\tau \\ &= \mathbf{\Phi}(\Delta t)\mathbf{x}((k-1)\Delta t) + \left(\int_{(k-1)\Delta t}^{k\Delta t} \mathbf{\Phi}(t-\tau)\,\mathrm{d}\tau\right)\mathbf{B}\mathbf{u}(k\Delta t) \\ &= \mathbf{\Phi}(\Delta t)\mathbf{x}((k-1)\Delta t) + \left(\int_0^{\Delta t} \mathbf{\Phi}(\tau)\,\mathrm{d}\tau\right)\mathbf{B}\mathbf{u}(k\Delta t)) \end{aligned} \tag{23}$$

The output equation is

$$\mathbf{y}(k\Delta t) = \mathbf{C}\mathbf{x}(k\Delta t) + \mathbf{D}\mathbf{u}(k\Delta t) \tag{24}$$

DOI: 10.1002/fld

Comparing to Equation (21), appropriate matrices for a discrete system are

$$\begin{aligned}\tilde{\mathbf{A}} &= \mathrm{e}^{\mathbf{A}\Delta t}\\ \tilde{\mathbf{B}} &= \left(\int_0^{\Delta t} \mathrm{e}^{\mathbf{A}\tau}\,\mathrm{d}\tau\right)\mathbf{B} = \mathbf{A}^{-1}(\mathrm{e}^{\mathbf{A}\Delta t} - \mathbf{I})\mathbf{B}\\ \tilde{\mathbf{C}} &= \mathbf{C}\\ \tilde{\mathbf{D}} &= \mathbf{D}\end{aligned} \tag{25}$$

The set of equations (21) has the same form as Equation (8) and can be modified as in Equation (10). The solution is then given by

$$\tilde{y}_k^m = \sum_{n=0}^{k} \tilde{\mathbf{H}}(k-n)\tilde{\mathbf{u}}_n \tag{26}$$

where for a unit sample input on the ith component of $\tilde{\mathbf{u}}$ the output response is $\tilde{H}^i$ the ith column of matrix $\tilde{\mathbf{H}}$.

For the discrete finite difference scheme used in the CFD code, information is only available about the solution at discrete intervals in time. If at these points in time it is assumed that the discrete system output matches the output of the continuous time scheme (i.e. the error is small and can be neglected), then the finite difference scheme is essentially the same as the scheme described in this section. Therefore the inverse of the transformation used here can be used on the matrices of the ROM obtained from the finite difference scheme.

Since the triple $[\tilde{\mathbf{A}}, \tilde{\mathbf{B}}, \tilde{\mathbf{C}}]$ is not unique (see Section 4), the triple where the matrix $\tilde{\mathbf{A}}$ is diagonal is taken to simplify the inversion process. Diagonalization of $\tilde{\mathbf{A}}$ is easily achievable for the problems discussed in this paper and the continuous-system matrices are then given by

$$\begin{aligned}\mathbf{A} &= \ln(\tilde{\mathbf{A}})/\Delta t\\ \mathbf{B} &= (\tilde{\mathbf{A}} - \mathbf{I})^{-1}\mathbf{A}\tilde{\mathbf{B}}\\ \mathbf{C} &= \tilde{\mathbf{C}}\\ \mathbf{D} &= \tilde{\mathbf{D}}\end{aligned} \tag{27}$$

6. TEST CASE INPUT CHANNELS

The methods described in Sections 5.1 and 5.2 will be applied to the identification of a continuous ROM for the flow about an aerofoil with trailing edge flaps that can undergo linearized pitch motions. For this motion, the position of a point on the aerofoil surface at any time is

$$\begin{aligned}x(t) &= \overline{x} + \Delta x(t)\\ y(t) &= \overline{y} + \Delta y(t)\end{aligned} \tag{28}$$

DOI: 10.1002/fld

Table I. Channel inputs to linearized Euler equations for linearized pitch and flap motions.

	Channel 1 α $(t = k\Delta t)$	Channel 2 δ $(t = k\Delta t)$	Channel 3 $\dot{\alpha}$ $(t = k\Delta t)$	Channel 4 $\dot{\delta}$ $(t = k\Delta t)$	All channels $\alpha, \delta, \dot{\alpha}, \dot{\delta}$ $(t \neq k\Delta t)$
Δx	$(\overline{y} - b_c)c_1$	$(\overline{y} - h_y)c_2$	0	0	0
Δy	$-(\overline{x} - a_c)c_1$	$-(\overline{x} - h_x)c_2$	0	0	0
x_t	0	0	$(\overline{y} - b_c)c_3$	$(\overline{y} - h_y)c_4$	0
y_t	0	0	$-(\overline{x} - a_c)c_3$	$-(\overline{x} - h_x)c_4$	0

$\Delta x, \Delta y$ are displacements and x_t, y_t are grid speeds of a point on the aerofoil.

where $\overline{x}, \overline{y}$ are the mean steady position of the point on the aerofoil surface and $\Delta x, \Delta y$ are the displacements of the point at time t. The displacements are given by

$$\begin{aligned} \Delta x &= (\overline{y} - b_c)\alpha_{\text{amp}}(t) + S(h_x)(\overline{y} - h_y)\delta(t) \\ \Delta y &= -(\overline{x} - a_c)\alpha_{\text{amp}}(t) - S(h_x)(\overline{x} - h_x)\delta(t) \end{aligned} \tag{29}$$

and the grid speed of the point on the aerofoil surface x_t, y_t are given by

$$\begin{aligned} \dot{x} &= (\overline{y} - b_c)\dot{\alpha}_{\text{amp}}(t) + S(h_x)(\overline{y} - h_y)\dot{\delta}(t) \\ \dot{y} &= -(\overline{x} - a_c)\dot{\alpha}_{\text{amp}}(t) - S(h_x)(\overline{x} - h_x)\dot{\delta}(t) \end{aligned} \tag{30}$$

where (h_x, h_y) is the hinge location and

$$\begin{aligned} S(h_x) &= 0 \quad \overline{x} < h_x \\ S(h_x) &= 1 \quad \overline{x} \geqslant h_x \end{aligned}$$

There are four associated input channels for this flow. the pulse inputs are given in Table I. The scaling constants $c_1, \ldots, c_4$ are used to reduce the number of subiterations needed to achieve a given error level and to avoid the sum of the mean value and the perturbation in wall pressure becoming negative.

7. RESULTS

The test cases shown here are for a NACA0012. The grid used for the calculations is of size 191×36, this means that the number of unknowns is 26 600. A steady calculation is performed for the aerofoil at incidence $\alpha = 0°$. The steady flow pressure distributions at freestream Mach numbers $M = 0.7$ and 0.80 are shown in Figure 1. These Mach numbers have been selected to illustrate flows without and with shockwaves.

It should be noted that the main costs associated with the present approach are the unsteady CFD calculations needed to find the pulse responses of the code. The additional costs for ERA and inversion are negligible in comparison. The number of pulse response calculations depends on the number of system inputs, so the costs of the method increase as the number of inputs increases and is related to the efficiency of the CFD code used.

DOI: 10.1002/fld

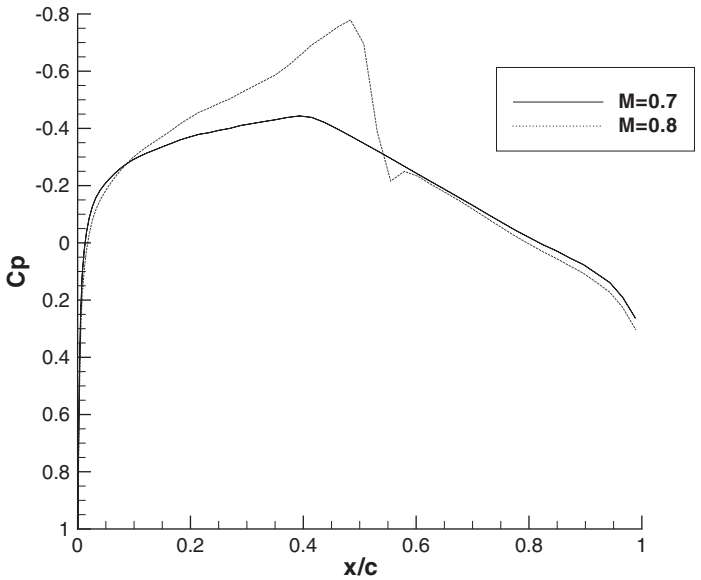

Figure 1. Steady pressure distributions $M = 0.7, 0.8$.

Table II. Channel inputs to the linearized Euler equations for linearized pitch and linearized flap motions.

M	Δt_1	c_1	c_2	c_3	c_4
0.7	0.2608	$\pi/180$	$\pi/180$	$0.335\pi/180$	$0.335\pi/180$
0.8	0.2282	$\pi/180$	$\pi/180$	$0.382\pi/180$	$0.382\pi/180$

7.1. Procedure for ROM generation

The procedure to generate continuous ROMs starts with the calculation of the sample responses of the CFD scheme for each input. The non-dimensional time step used is $\Delta t_1 = (\Delta t_1^{dim}/c)\sqrt{p_\infty/\rho_\infty}$ where the time step Δt_1^{dim}, freestream speed of sound c, freestream pressure p_∞ and freestream density ρ_∞ are all dimensional quantities. The values of the time step and input scaling constants for the two Mach numbers under consideration are shown in Table II. As an example, the sample responses for each of the four input channels are shown for $M = 0.7$ in Figure 2.

The ERA algorithm was then used to produce a discrete ROM from the sample responses at each Mach number. Two continuous ROMs are then generated using the methods described in Sections 5.1 and 5.2.

The first continuous ROM, produced by inverting the implicit transformation, is put into discrete form for calculations using the implicit scheme. ROM solutions produced are labelled imp in all figures.

The second continuous ROM, produced using the inverse sampling approach, is put into discrete form for calculations in two ways. ROM solutions produced by putting the equations into discrete form using the implicit scheme are labelled sp-imp and ROM solutions produced by putting the

DOI: 10.1002/fld

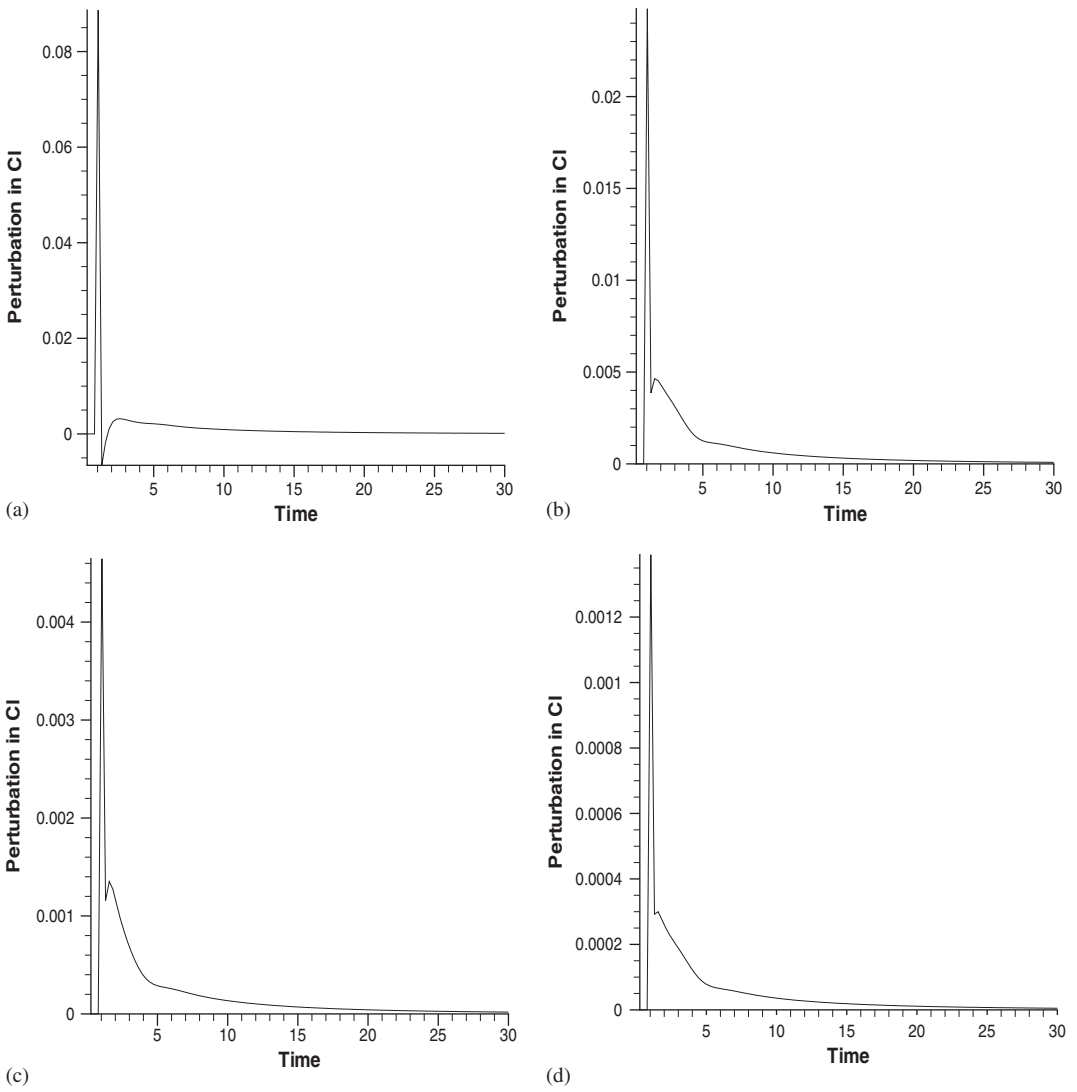

Figure 2. Example pulse responses $M = 0.7$: (a) α; (b) δ; (c) $\dot{\alpha}$; and (d) $\dot{\delta}$.

equations into discrete form using the inverse sampling scheme are labelled sp-sp. For the $M = 0.7$ case, the ROM used in this investigation has rank 17 and for $M = 0.8$ the ROM has rank 21.

7.2. Sinusoidal linear pitch oscillations

The pitch motion is defined in dimensional variables by

$$\alpha_{\text{amp}}(t) = \alpha_{\max} \sin(\omega t) \tag{31}$$

DOI: 10.1002/fld

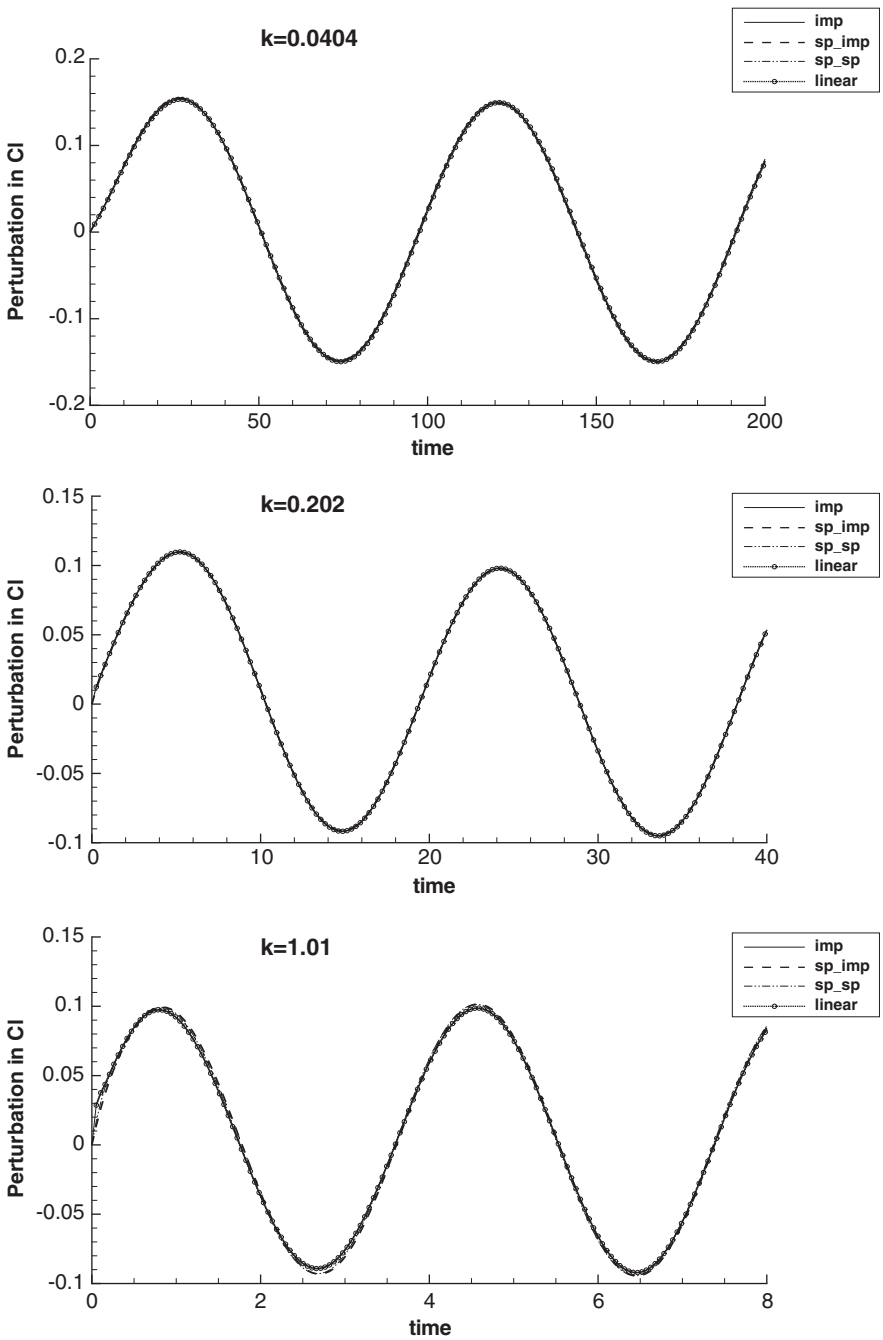

Figure 3. Lift perturbation for pitch oscillations at three frequencies, $M = 0.7$.

DOI: 10.1002/fld

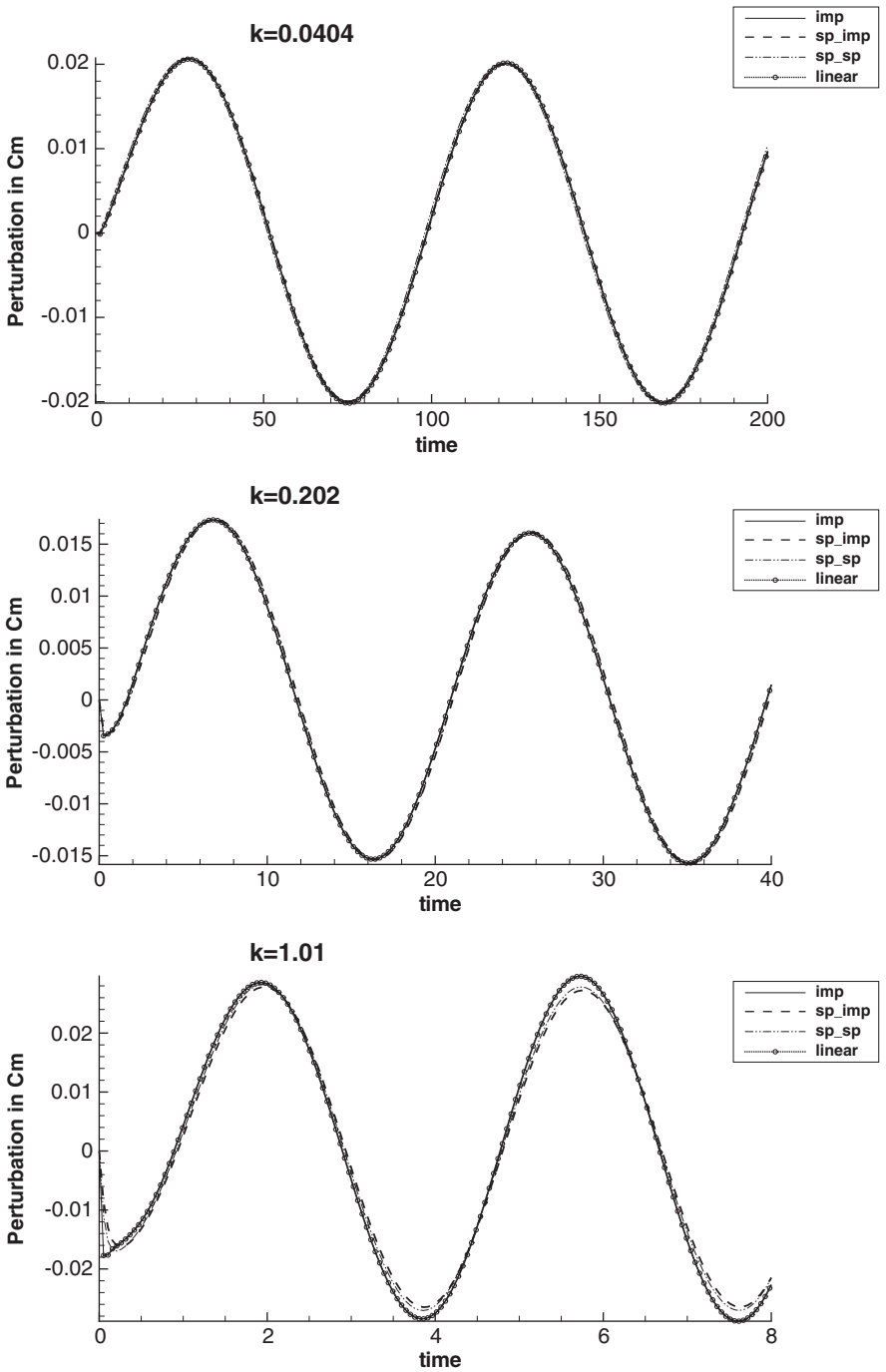

Figure 4. Moment perturbation for pitch oscillations at three frequencies, $M = 0.7$.

DOI: 10.1002/fld

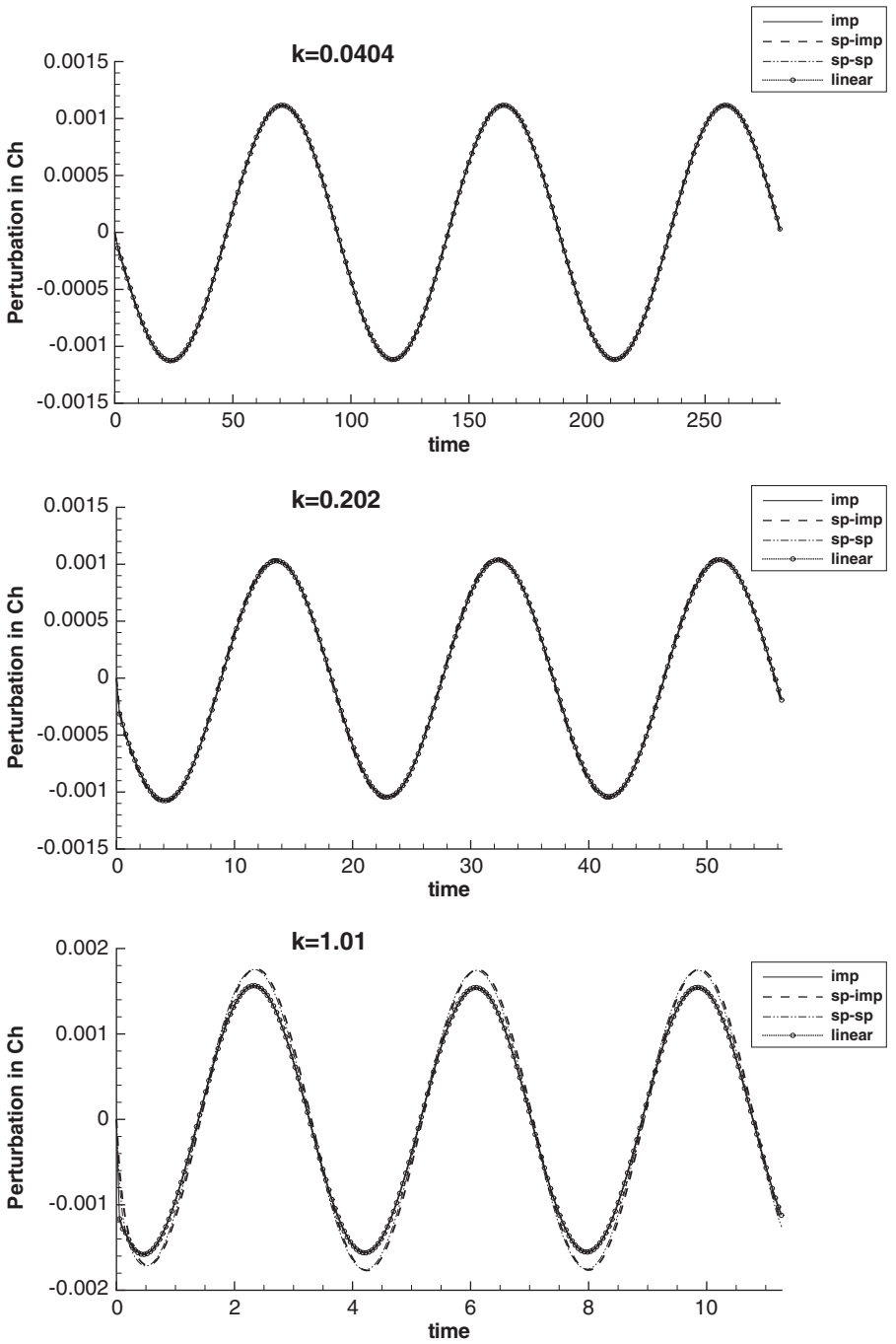

Figure 5. Hinge moment perturbation for pitch oscillations at three frequencies, $M = 0.7$.

DOI: 10.1002/fld

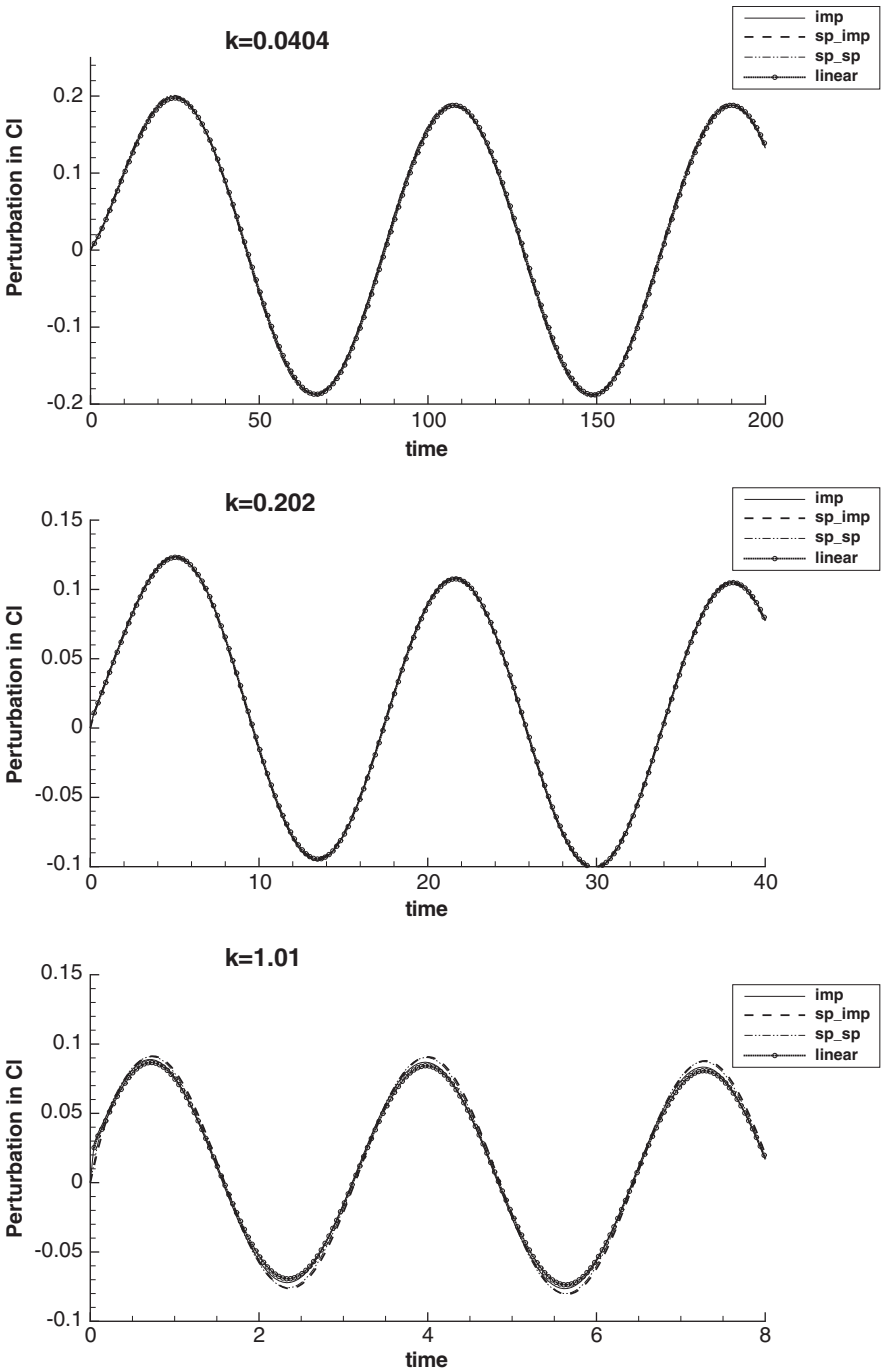

Figure 6. Lift perturbation for pitch oscillations at three frequencies, $M = 0.8$.

DOI: 10.1002/fld

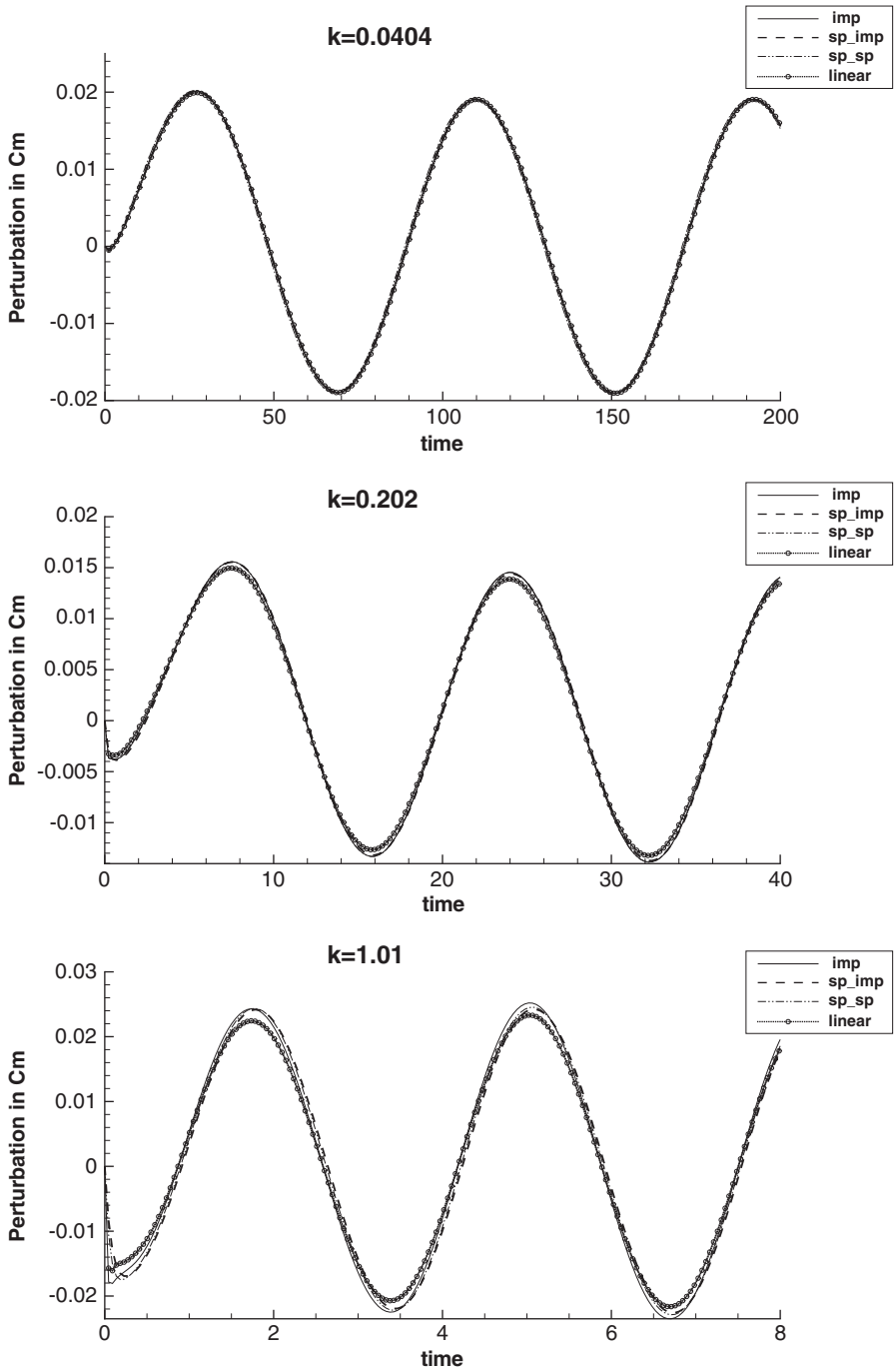

Figure 7. Moment perturbation for pitch oscillations at three frequencies, $M = 0.8$.

DOI: 10.1002/fld

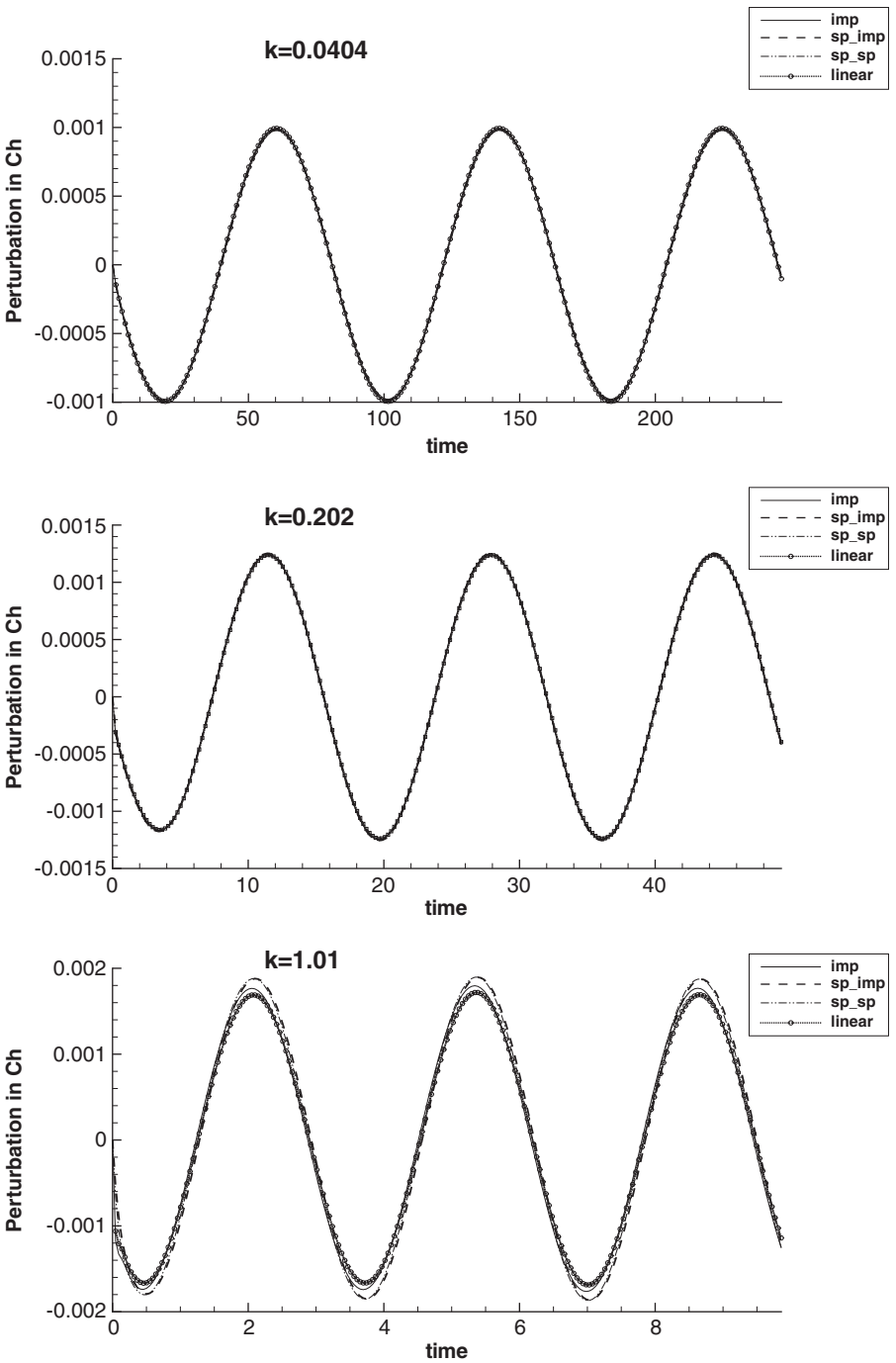

Figure 8. Hinge moment perturbation for pitch oscillations at three frequencies, $M = 0.8$.

DOI: 10.1002/fld

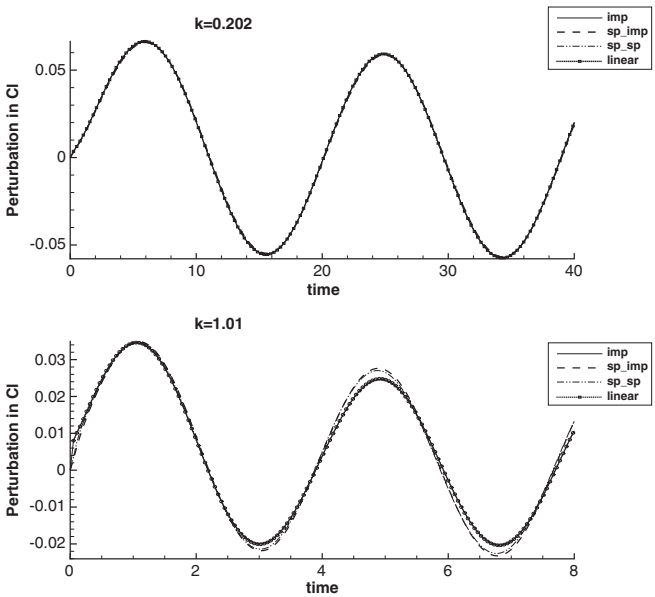

Figure 9. Lift perturbation for flap oscillations at two frequencies, $M = 0.7$.

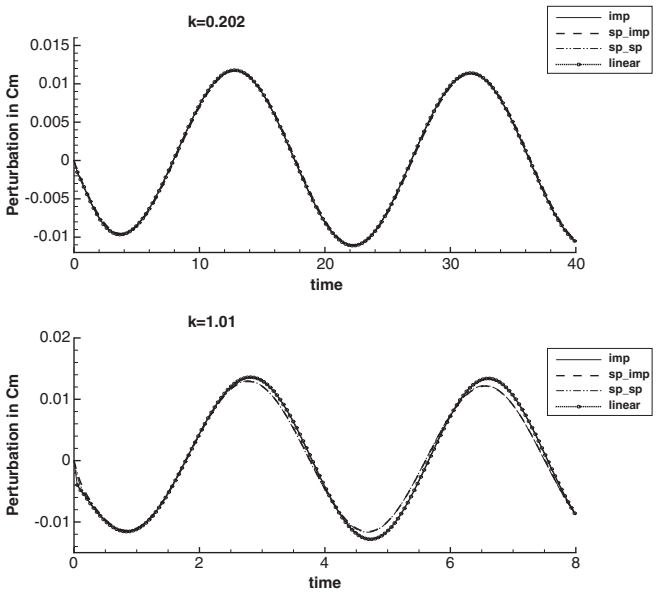

Figure 10. Moment perturbation for flap oscillations at two frequencies, $M = 0.7$.

DOI: 10.1002/fld

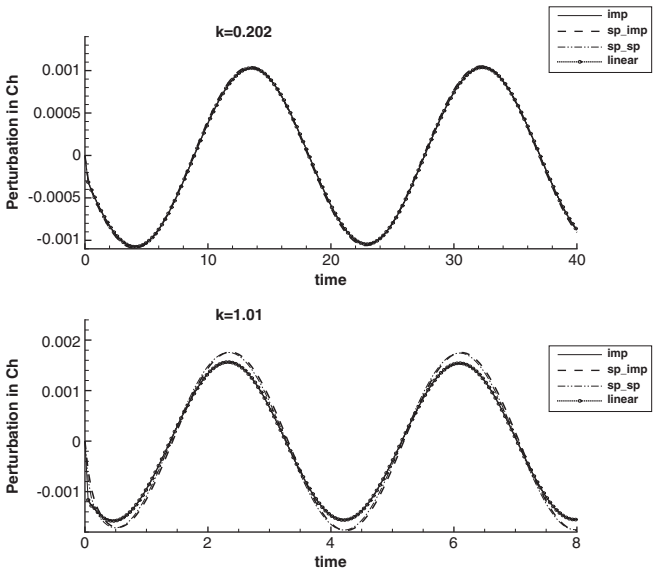

Figure 11. Hinge moment perturbation for flap oscillations at two frequencies, $M = 0.7$.

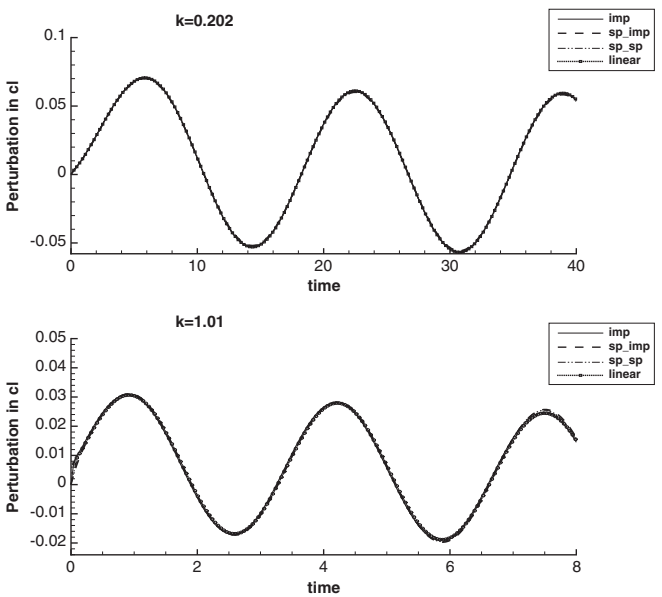

Figure 12. Lift perturbation for flap oscillations at two frequencies, $M = 0.8$.

DOI: 10.1002/fld

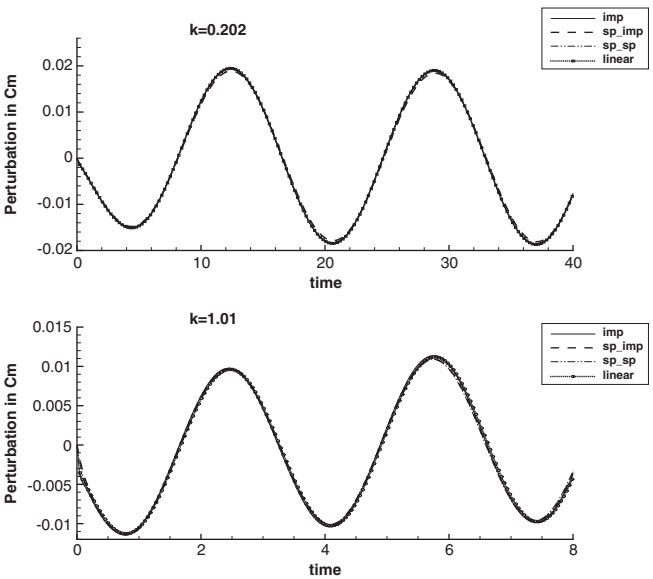

Figure 13. Moment perturbation for flap oscillations at two frequencies, $M = 0.8$.

where ω is related to the non-dimensional reduced frequency, k_{red} via

$$k_{\text{red}} = \frac{\omega c}{2U_\infty} \tag{32}$$

Calculations were performed with $\alpha_{\max} = 1^{\text{o}}$ at $M = 0.7, 0.8$ for three reduced frequencies $k_{\text{red}} = 0.0404, 0.202, 1.01$. Each calculation was performed with 72 steps per period. At the three frequencies, the non-dimensional time steps are $5\Delta t_1$, Δt_1, $\Delta t_1/5$, respectively, where the continuous ROM was created using a pulse width of Δt_1. Solutions for $M = 0.7$ are shown in Figures 3–5. The full linear solution, labelled *linear* is compared with the three ROM solutions. The figures show that lift, pitch moment and hinge moment for all solutions are in good agreement at the medium and low frequencies. At the higher frequency the lift solutions are in good agreement, but the two inverse sampling-based ROM solutions exhibit small errors in amplitude compared to the full linear solution in pitching moment and hinge moment. The implicit ROM solution is still in good agreement with the full solution.

Solutions for $M = 0.8$, where the mean flow has a shock, are shown in Figures 6–8. The lowest frequency solutions show good agreement between all the methods for both lift, pitching moment and hinge moment. At the medium frequency the lift and hinge moment values are in agreement, but all three ROMs show a small error in pitching moment. The ROM solutions labelled imp and sp-sp overlay as expected since the medium frequency solutions are calculated using the same time step as used to obtain the pulse responses. This means both calculations should have the same discrete system form. At the higher frequency the inverse sampling-based ROM solutions have errors in lift, pitching moment and hinge moment. The implicit-based ROM has good agreement in lift and small errors in pitching and hinge moments.

DOI: 10.1002/fld

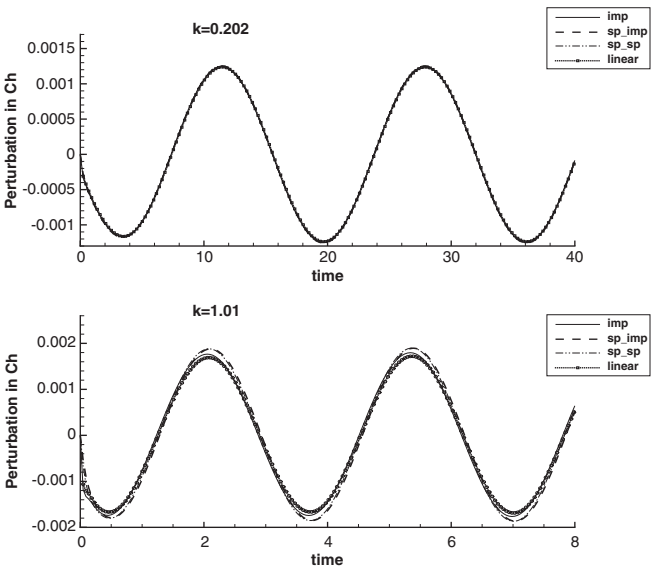

Figure 14. Hinge moment perturbation for flap oscillations at two frequencies, $M = 0.8$.

7.3. Sinusoidal linear flap oscillations

The flap motion is defined in dimensional variables by

$$\delta_{\text{amp}}(t) = \delta_{\max} \sin(\omega t) \tag{33}$$

Calculations are performed for the same frequencies and Mach numbers as for linear pitch, with a maximum flap angle $\delta_{\max} = 1^{\text{o}}$. Solutions for the lowest frequency are not shown as all ROM solutions are in excellent agreement with the full solution in lift, pitching moment and hinge moment.

Solutions for $M = 0.7$ are shown in Figures 9–11. At the medium frequency, all solutions are in excellent agreement with the full solution. However, at the higher frequency the implicit ROM solution has good agreement, but the two inverse sampling-based ROM solutions show a small error in the solution in lift, pitching moment and hinge moment.

Solutions for $M = 0.8$ are shown in Figures 12–14. Again good agreement is seen at the medium frequency, with small errors in the inverse sampling-based results at the higher frequency.

7.4. Further investigations

The trends from the test cases considered above is that as the frequency is increased, small errors start to be observed between the full linear solution and the ROM solutions, particularly those produced from a continuous ROM obtained using the sampling inversion technique. A further investigation was thus carried out for one case, that of a pitching aerofoil at $M = 0.7$. Additional solutions were calculated with $k_{\text{red}} = 2.02$, 4.04, 8.08, 10.1 and 20.2. The number of steps per cycle was kept at 72 as for all the testcases in previous sections. Thus the corresponding time steps are $\Delta t_1/10$, $\Delta t_1/20$, $\Delta t_1/40$, $\Delta t_1/50$ and $\Delta t_1/100$. Figure 15 shows the moment perturbation as it was

DOI: 10.1002/fld

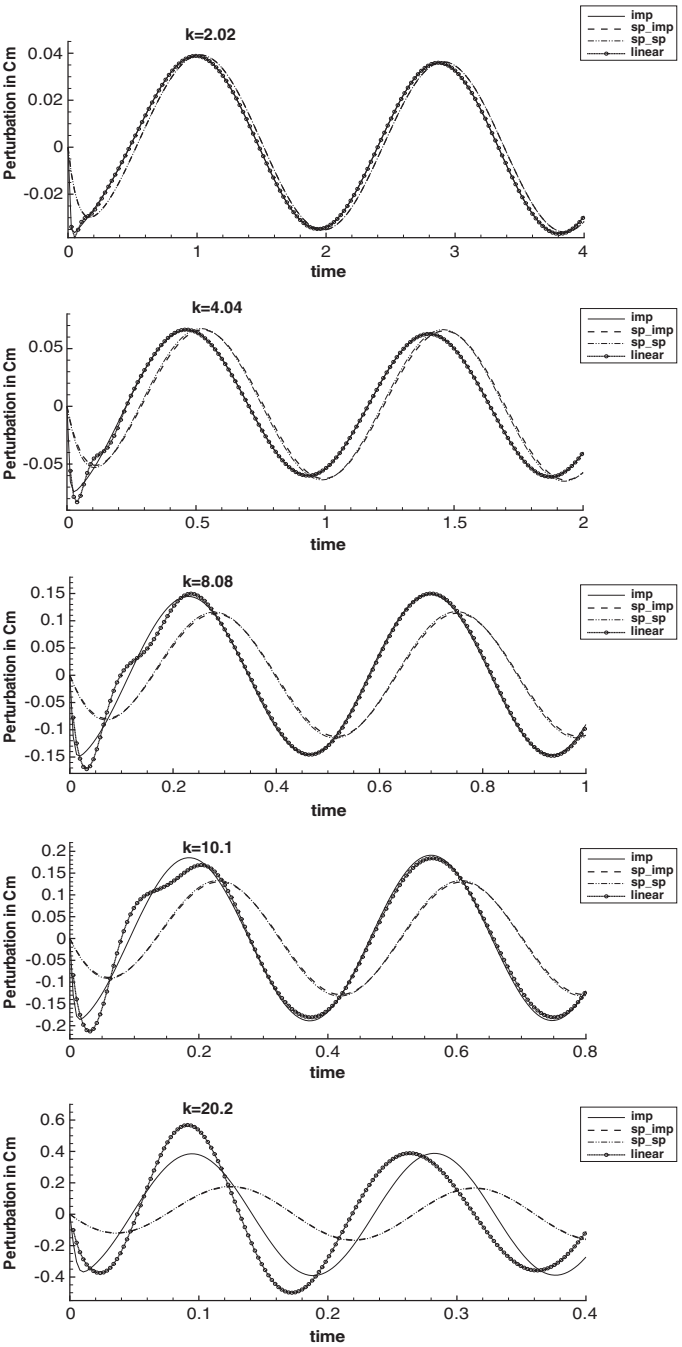

Figure 15. Higher frequency moment perturbations at $M = 0.7$.

DOI: 10.1002/fld

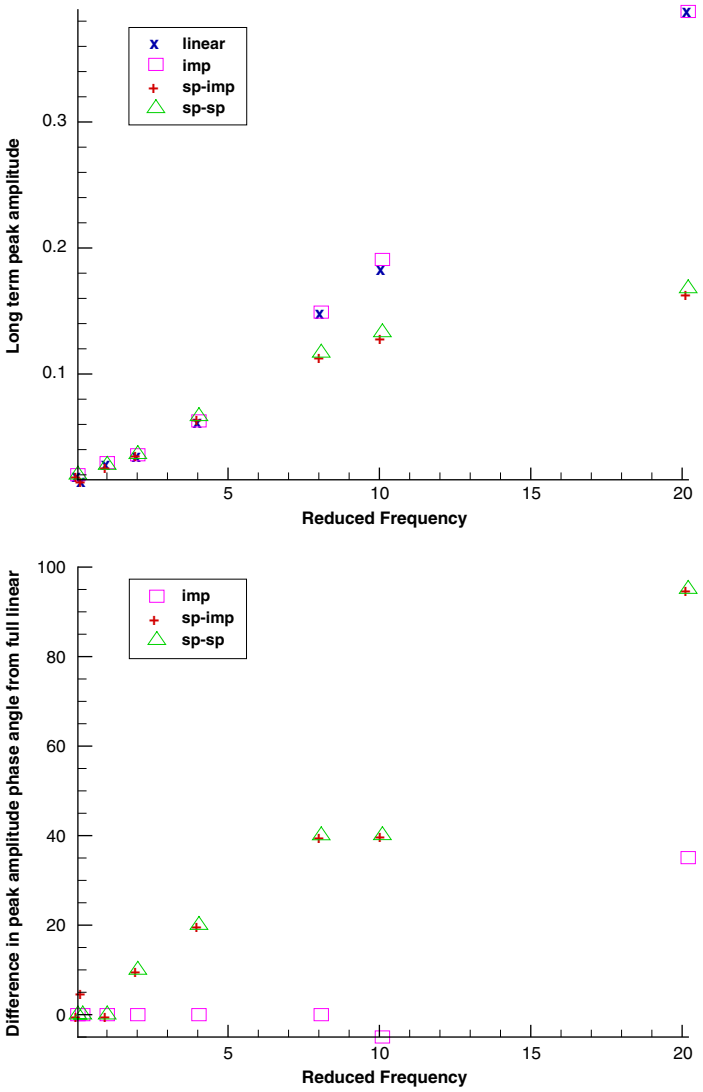

Figure 16. Long-term moment peak amplitude and its location.

most sensitive to frequency. Also shown in Figure 16 is the long-term peak amplitude and the difference in the phase angle at which this peak is located compared with the full linear solution. It can be seen that significant errors develop in the sampling-based ROM solutions compared to the full linear solution from $k_{\text{red}} = 4.04$ onwards. The implicit ROM solution performs better. The initial transient is less well predicted for reduced frequencies above $k_{\text{red}} = 4.04$, but good predictions of the long-term sinusoidal behaviour are maintained right up to $k_{\text{red}} = 10.1$. At this frequency, the period of motion is less than $2\Delta t_1$. Note it is inevitable that the implicit scheme eventually begins to become unable to capture the initial transient and eventually the long-term sinusoidal behaviour

DOI: 10.1002/fld

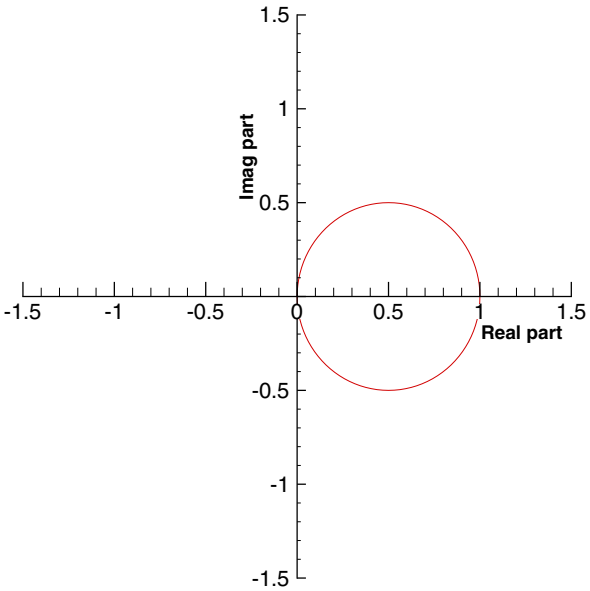

Figure 17. Discrete eigenvalue space showing map of stable continuous system.

as the frequency increases. This is because for these cases, very high frequency terms are important and these are not the dominant terms of the full linear system for the time step used to create the ROM. These terms are therefore not identified by the ERA scheme.

To investigate the differences in behaviour of the two methods, the effect of the mappings on the reduced system eigenvalues is considered. The reduced-order continuous scheme is stable if its eigenvalues have positive real part and so the corresponding discrete implicit scheme must have eigenvalues lying within the circle shown in Figure 17. The discrete ROMs yielded by the identification scheme have eigenvalues lying within the required circle.

An eigenvalue, $\lambda = \lambda_r + \mathrm{i}\lambda_i$, of the reduced-order continuous-system matrix A and the corresponding eigenvalue, $\tilde{\lambda} = \tilde{\lambda}_r + \mathrm{i}\tilde{\lambda}_i$, of the reduced-order discrete system matrix $\tilde{A}$ are related via

$$\lambda = \frac{\tilde{\lambda} - 1}{\tilde{\lambda}\Delta t} \tag{34}$$

for the simple implicit inversion scheme and

$$\lambda = \frac{\ln(\tilde{\lambda})}{\Delta t} \tag{35}$$

for the sampling-based processing inversion scheme. Since both methods start from the same discrete ROM, the differences are related to these mappings rather than to what has been identified by the ERA algorithm.

The differences between these mappings when it is applied to an array of points lying within the circle of Figure 17 are shown in Figures 18 and 19. These show the difference in magnitude and phase angle for the continuous eigenvalues mapped using the implicit and sampling-based

DOI: 10.1002/fld

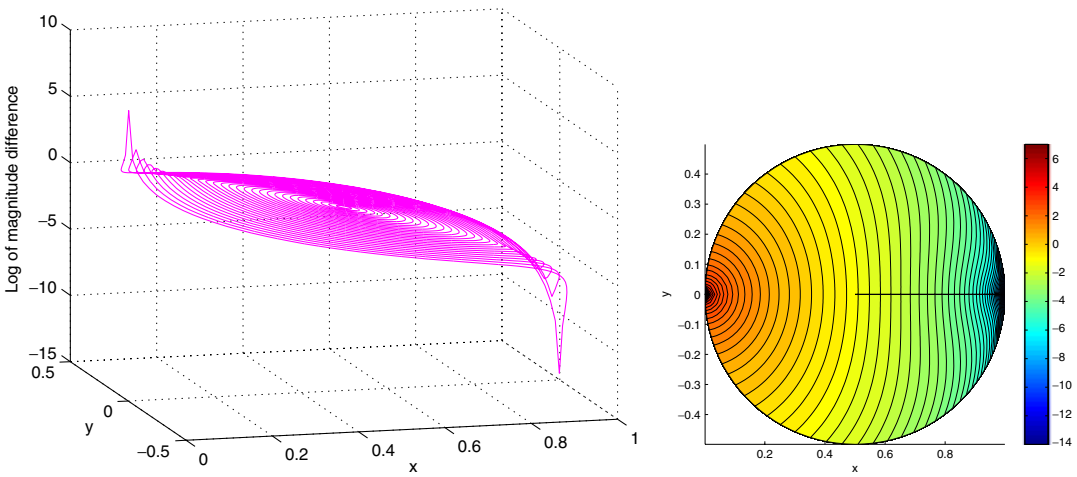

Figure 18. Log of the difference in magnitude of the continuous eigenvalues for the two mappings.

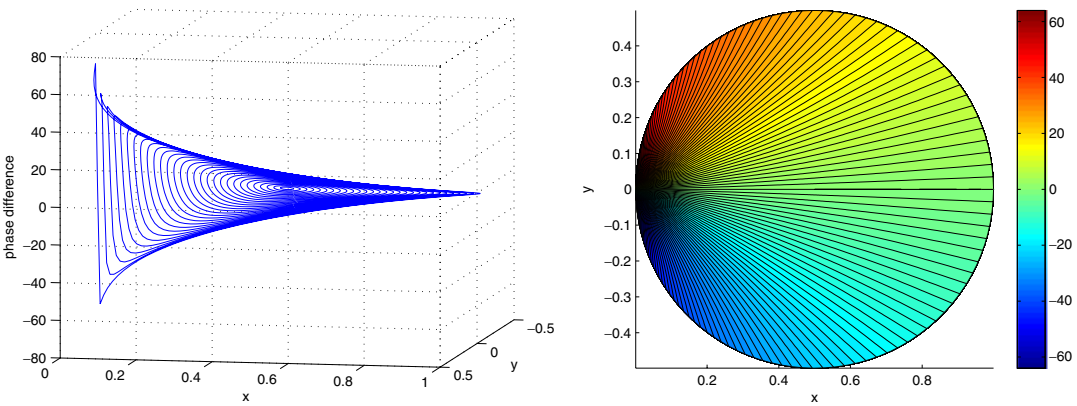

Figure 19. Difference in phase angle (in degrees) of the continuous eigenvalues for the two mappings.

schemes. The greatest differences are found for discrete eigenvalues with the smallest real parts. The discrete eigenvalues nearest to the origin have a significant influence at higher frequencies, but are less important at lower frequencies. Hence there are bigger differences between the implicit and sampling-based ROM solutions at higher frequencies. From the results it seems that the implicit ROM is more appropriate at higher frequencies.

7.5. Example aeroelastic application

The focus of this paper is on continuous ROMs of the fluid motion. The ultimate application of these models is for aeroelastic calculations including those with structural non-linearities. To demonstrate that the ROMs can indeed be used in place of full CFD solutions, an illustrative test case is presented. The example system used is a three-degree-of-freedom system for a NACA64A010

DOI: 10.1002/fld

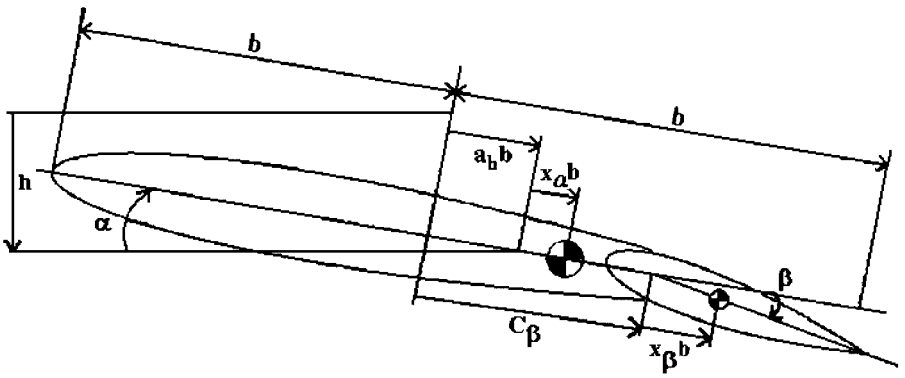

Figure 20. A three-degree-of-freedom aeroelastic system.

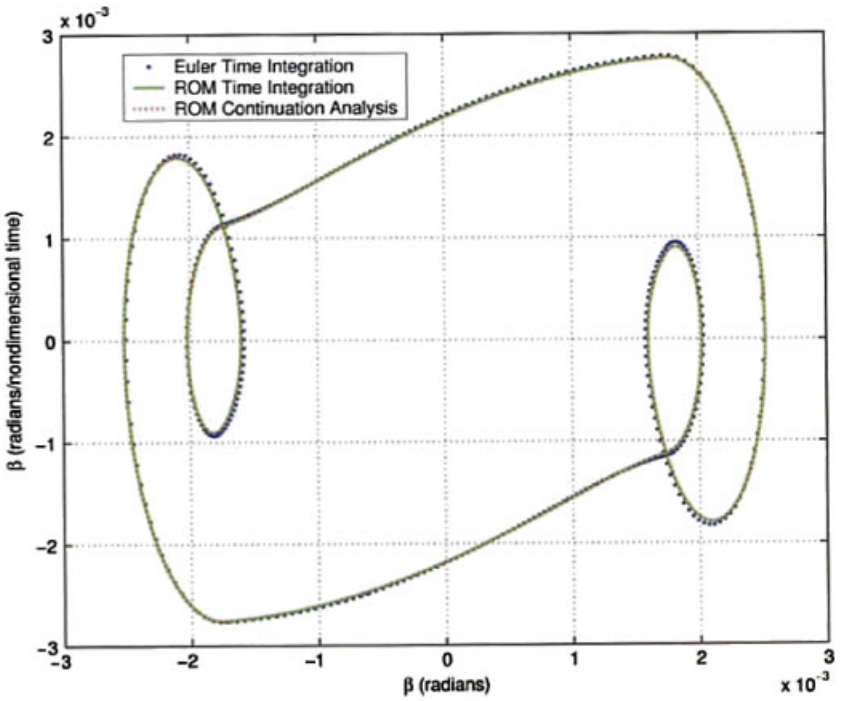

Figure 21. Example aeroelastic solution.

aerofoil; with vertical heave translation, rotational pitch and control surface pitch motion, see Figure 20. The usual linear structural model, obtained if there is no structural damping, is modified so that the stiffness constants are functions of displacement and velocity. The example result, shown here, is for a freeplay of amplitude 0.1° in the flap stiffness which is a function of displacement. Figure 21 shows a phase plane plot (δ vs $\dot{\delta}$) for a limit cycle; the free stream Mach number is

DOI: 10.1002/fld

$M_\infty = 0.845$ and the flutter speed index is $U_* = 0.176$. The full CFD solutions were obtained from a time-accurate version of Jameson's standard cell-centred finite volume scheme adapted for moving meshes. Good agreement is found between ROM and full CFD solutions. Further results for this and other test cases can be found in Reference [33].

8. CONCLUSIONS

Two different methods for deriving a continuous ROM from a discrete ROM, obtained from the pulse responses of a linear CFD code, have been investigated. The results shown indicate that both the continuous ROMs are able to reproduce the full linear solution for sinusoidal motions at the lower frequencies, where a time step close to that used to calculate the pulse responses is appropriate. As the frequency is increased and the time step is decreased, the sampling-based inversion method showed errors at a much lower frequency than the implicit inversion technique. This is due to the fact that the eigenvalues of the continuous ROM corresponding to the higher frequency terms are less accurately mapped by the sampling-based inversion transformation.

Thus using a sampling-based approach even when it has not been used to put a system into discrete form can be an appropriate way to generate a continuous ROM. It should be noted, however, that its range of applicability will be limited.

REFERENCES

1. Venkatakrishnan V, Jameson A. Computation for unsteady transonic flows by the solution of the Euler equations. *AIAA Journal* 1998; **26**:974–981.
2. Brenneis A, Erbele A. Evaluation of an unsteady implicit Euler code against two and three-dimensional standard configurations. *AGARD CP-507*, 1991; Paper 10.
3. Guruswamy GP. Unsteady aerodynamic and aeroelastic calculations for wings using Euler equations. *AIAA Journal* 1990; **28**:461–469.
4. Jameson AJ. Time dependent calculations using multigrid, with applications to unsteady flows past airfoils and wings. *AIAA Paper 91-1596*, 1991.
5. Gaitonde AL. A dual time method for the solution of the unsteady Euler equations. *Aeronautical Journal* 1994; **98**(978):283–291.
6. Dowell EH, Hall KC. Modelling of fluid-structure interation. *Annual Review of Fluid Mechanics* 2001; **33**: 445–490.
7. Juang J-N, Pappa RS. An eigensystem realization algorithm for modal parameter identification and model reduction. *Journal of Guidance, Control and Dynamics* 1985; **8**(5):620–627.
8. Ho BL, Kalman RE. Effective construction of linear state-variable models from input/output functions. *Regelungstechnik* 1966; **12**(14):545–548.
9. A survey of model reduction methods for large systems. *Contemporary Mathematics* 2001; **280**:193–219. AMS Publications: Providence, RI. Technique for unsteady transonic aerodynamic flows. *AIAA Journal* 2000; **38**(10):1853–1862.
10. Grimme EJ. Krylov projection methods for model reduction. *Ph.D. Thesis*, University of Illinois, Urbana-Champagne, 1997.
11. Willcox KE. Reduced-order aerodynamic models for aeroelastic control of turbomachines. *MIT Thesis*, 2000.
12. Chen J, Kang S, Zou J, Liu C, Schutt-Aine JE. Reduced-order modeling of weakly non-linear MEMS devices with Taylor-series expansion and Arnoldi approach. *Journal of Microelectromechanical Systems* 2004; **13**(3):441–451.
13. Romanowski MC. Reduced order unsteady aerodynamic and aeroelastic models using Karhunen–Loeve eigenmodes. *Proceedings of the Sixth AIAA Symposium on Multidisciplinary Analysis and Optimization 1996*, *AIAA Paper 96-3981*, 1996.
14. Romanowski MC, Dowell EH. Reduced order Euler equations for unsteady aerodynamic flows: numerical techniques. *AIAA Paper 96-0528*, 1996.

DOI: 10.1002/fld

15. Hall KC, Thomas JP, Dowell EH. Reduced-order modeling of unsteady small disturbance flows using a frequency domain proper orthogonal decomposition technique. *AIAA Paper 99-0655*, 1999.
16. Hall KC, Thomas JP, Dowell EH. Proper orthogonal decomposition technique for transonic unsteady aerodynamic flows. *AIAA Journal* 2000; **38**(10):1853–1862.
17. Willcox K, Peraire J. Balanced model reduction via proper orthogonal decomposition. *AIAA Paper 2001-2611*, 2001.
18. Raveh DE. Reduced-order models for nonlinear unsteady aerodynamics. *AIAA Journal* 2001; **39**(8):1417–1429.
19. Silva WA. Discrete-time linear and nonlinear aerodynamic impulse responses for efficient CFD analyses. *Ph.D. Thesis*, Department of Applied Science, College of William and Mary, Virginia, U.S.A., 1997.
20. Gaitonde AL, Jones DP. System identification and reduction from the pulse responses of a linearised Euler scheme. *CEAS Aerospace Aerodynamics Research Conference*, Cambridge, 2002.
21. Antoulas AC, Sorensen DC, Gugercin S. A survey of model reduction methods for large-scale systems. *Contemporary Mathematics* 2001; **280**:193–219.
22. Antoulas AC. Approximation of large-scale dynamical systems. *Advances in Design and Control* 2005.
23. Tang D, Kholodar D, Juang J-N, Dowell EH. System identification and proper orthogonal decomposition method applied to unsteady aerodynamics. *AIAA Journal* 2001; **39**(8):1569–1576.
24. Roberts I, Gaitonde AL, Jones DP, Lieven NAJ. Identification of limit-cycles for piecewise nonlinear aeroelastic systems in transonic regimes. *CEAS Aerospace Aerodynamics Research Conference*, Cambridge, 2002.
25. Gaitonde AL, Jones DP. Solutions of the 2D linearised unsteady Euler equations on moving meshes. *Proceedings of the Institution of Mechanical Engineering*, vol. 216, Part G. *Journal of Aerospace Engineering* 2002;89–104.
26. Gaitonde AL, Jones DP. The use of pulse responses for 2D unsteady flows and system reduction. *Aeronautical Journal* 2002;483–492.
27. Gaitonde AL, Jones DP. Reduced order state-space models from the pulse responses of a linearised CFD scheme. *International Journal for Numerical Methods in Fluids* 2003; **42**:581–606.
28. Aplevich JD. *The Essentials of Linear State-Space Systems*. Wiley: New York, 2000.
29. Gaitonde AL, Jones DP. Study of linear response identification techniques and reduced order model generation for a 2D CFD scheme. *International Journal for Numerical Methods in Fluids* 2006, accepted.
30. Doetsch G. *Guide to the Application of the Laplace and Z-Transforms* (2nd edn). Van Nostrand Reinhold Company: New York, 1971.
31. McGillem CD, Cooper GR. *Continuous and Discrete Signal and System Analysis*. CBS Publishing Japan Ltd, 1984.
32. Lucia DJ, Beran PS, Silva WA. Aeroelastic system development using proper orthogonal decomposition and volterra theory. *AIAA Paper 2003-1922*, 2003.
33. Roberts I, Gaitonde AL, Lieven NAJ, Jones DP. Identification of limit cycles for piecewise nonlinear aeroelastic systems in transonic regimes. *AIAA CFD Conference*, Toronto, June 2005.

DOI: 10.1002/fld